Design of an SDOF system with backlash

Design of an SDOF system with backlash

Master Team Project

Report No. DCT 2007.110

Students:	B.P.T. van Goch	0528204
	P.J. Neefs	0531682
	T.A.M. Wegman	0536193

Supervisor:	Prof. dr. H. Nijmeijer
Coaches:	Dr. ir. R.H.B. Fey
	P.W.C. van Hoof
	Ir. L. Kodde

Eindhoven University of Technology
Department of Mechanical Engineering
Dynamics and Control Group

Eindhoven, September 14, 2007

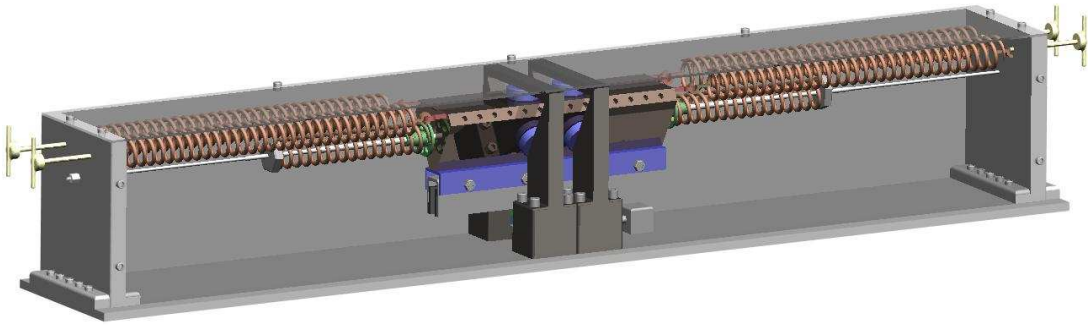

Overview of the SDOF system with backlash: final result of the design process.

Contents

Chapter 1

Introduction

In this report the design and construction of an experimental setup with backlash is considered. Backlash, dead zone or clearance is a common feature in many mechanical systems and can deteriorate the performance of the system. It can be caused by intended clearance necessary for assembly and operation, but may also be the result of operational wear and tear. Backlash has a large influence on the dynamics and control of systems such as power transmissions, robotics and measurement systems. For instance, it can lead to rattle and chaotic motion in gear systems, causing damage and noise. Systems with backlash form a subclass of discontinuous mechanical systems and can be modeled as piecewise linear systems [1].

Much theoretical research has been done on backlash. This report is inspired on the report of Besselink [1], in which extensive theoretical studies on systems with backlash have been done. However, instead of modeling such systems, this report focuses on the actual design and construction of a physical system with backlash. Using such an experimental setup, theoretical models and results can be validated experimentally.

This report is organized as follows: in chapter 2, the model of a system with backlash will be introduced. Furthermore, the desired behavior of the experimental setup (which is to be designed) will be described. Numerical methods for computing periodic solutions of the considered setup will be presented in chapter 3. Then, in chapter 4, the specific design of the different parts of the setup will be treated. The finally chosen parameters and accompanying dynamical behavior will be presented in chapter 5. Furthermore, in chapter 6 an alternative design will be given, where a different way of excitation is chosen.

Chapter 2

Modeling the experimental setup

In this chapter, a model of a single degree of freedom (SDOF) system with backlash will be presented. Furthermore, some choices on the dimensions and performance of the experimental setup will be made. With the previously found model [1], the dimensions of the setup will be chosen in such a way that the desired dynamical behavior will be present.

2.1 Model of an SDOF system with backlash

The aim of this study is to develop an experimental setup, inspired by Besselink [1]. The system as given in Besselink [1] is being considered first, see figure 2.1.

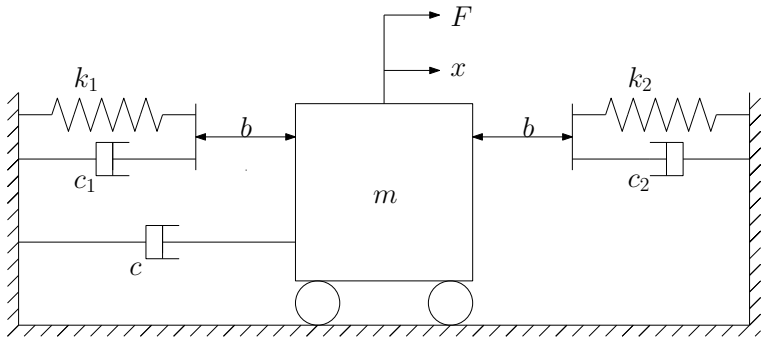

Figure 2.1: Schematic representation of the setup.

This system consists of a mass m that can move freely between two stoppers, which are positioned at a distance b from the mass. The mass is damped by a damper with damping constant c. Each of the stoppers can be viewed as a parallel system of one spring and one damper, with spring and damping constant $k_{1,2}$ and $c_{1,2}$ respectively. The mass of the stoppers is considered to be negligible. Furthermore, it is assumed that the stoppers are at rest in their initial positions, when contact with the mass takes place. Also, it is assumed that contact is lost if the the contact force between stopper and mass becomes zero. In this way, modeling the stopper dynamics is not necessary. Excitation of the system is done by prescribing a sinusoidal force F on the mass. These considerations lead to the following equation of motion:

$$m\ddot{x} + C(\dot{x}) + K(x) = F, \tag{2.1}$$

which can be given in a general first order form by:

$$\dot{\mathbf{x}} = \mathbf{f}(t, \mathbf{x}) \tag{2.2}$$

with $\mathbf{x} = [x, \dot{x}]^T$ and

$$\dot{\mathbf{x}} = \begin{bmatrix} \dot{x} \\ \frac{1}{m}(-C(\mathbf{x}) - K(\mathbf{x}) + F) \end{bmatrix} \tag{2.3}$$

The restoring force $K(\mathbf{x})$ and damping force $C(\mathbf{x})$ depend on the position and velocity of the mass. Therefore, the region of motion of the mass is divided into three subspaces V_1, V_2 and V_3, as shown in figure 2.2. The mathematical description reads:

$$K(\mathbf{x}) = \begin{cases} 0 & ,\mathbf{x} \in V_2; \\ k_1(x+b) & ,\mathbf{x} \in V_1; \\ k_2(x-b) & ,\mathbf{x} \in V_3; \end{cases} \tag{2.4}$$

$$C(\mathbf{x}) = \begin{cases} c\dot{x} & ,\mathbf{x} \in V_2; \\ (c+c_1)\dot{x} & ,\mathbf{x} \in V_1; \\ (c+c_2)\dot{x} & ,\mathbf{x} \in V_3; \end{cases} \tag{2.5}$$

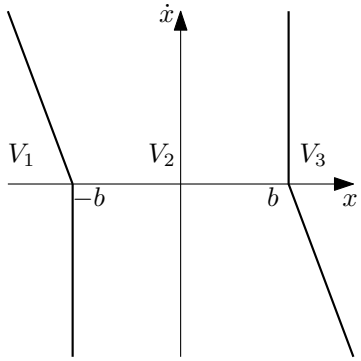

Figure 2.2: Subspaces of the SDOF system.

These subspaces are based on contact or no contact of the mass with the stoppers. The corresponding mathematical subspaces conditions are given by the following equations:

$$V_1 = \{x \in \mathbb{R}^2 \mid x < -b, k_1(x+b) + c_1\dot{x} \leq 0\} \tag{2.6}$$

$$V_3 = \{x \in \mathbb{R}^2 \mid x > b, k_2(x-b) + c_2\dot{x} \geq 0\} \tag{2.7}$$

$$V_2 = \{x \in \mathbb{R}^2 \mid x \notin (V_1 \cup V_3)\} \tag{2.8}$$

The latter corresponds to the case of no contact with the stoppers. In equation 2.6 and 2.7, it can be seen that the damping term is present for both positive and negative velocities. This is not realistic, since the mass is not attached to the stopper. Therefore it is not possible for the damper (of the stopper) to exert a force on the mass at the extension phase. With

a velocity dependent signum-function, the model would be more accurate. However, due to low damping forces ($\zeta \leq 2\%$) this phenomenon will be neglected. When a periodic excitation of the form given by:

$$F = Asin(2\pi ft) \tag{2.9}$$

is assumed, equation (2.2) becomes:

$$\dot{\mathbf{x}} = \begin{bmatrix} \dot{x} \\ \frac{1}{m}(-C(\mathbf{x}) - K(\mathbf{x}) + Asin(2\pi ft)) \end{bmatrix} \tag{2.10}$$

Equation 2.10 will be used later on to investigate the theoretical steady-state behavior of the system with backlash.

2.2 Design requirements for the experimental setup

The theoretical model described in the previous section, forms the basis for the design of the experimental setup. However, as long as there are no constraints on the design parameters, infinitely many solutions to the design problem exist. Therefore, in this section some limitations and desirable properties of the setup will be formulated.

2.2.1 Dimensions of the setup

Besides for experimental research on nonlinear dynamic systems, the setup is also designed for lecture room demonstration purposes. This means that portability is a very important requirement. Therefore, the maximal length, width and height are chosen to be about 1.0 m, 0.4 m and 0.4 m respectively. Since one operator must be able to lift and transport the setup by himself, the maximal weight is chosen to be approximately 30 kg.

The visibility of the movement of the mass is very important for demonstrations, so the backlash b is chosen to be 0.05 m. This implies that the mass should move 5 cm from its center position to hit a stopper.

2.2.2 Desired dynamics

As pointed out in figure 2.1, the freely movable mass m is excited by a sinusoidal forcing F, with frequency f. The following equation for the peak force, as a function of frequency, holds as long as long as the mass is in subspace V_2 (no contact with the stoppers):

$$F_{peak}(f) = 4mb\pi^2 f^2 cos(2\pi ft) + 2b\pi fC(\mathbf{x})sin(2\pi ft) \tag{2.11}$$

In (2.11), acceleration and velocity dependent force terms are present. For safety reasons, a maximal forcing amplitude of 30 N is taken. When neglecting damping terms, this means that for a mass of 1 kg and a backlash of b=0.05 m, the forcing is able to generate a maximal frequency of 3.89 Hz. As will be proven later, the actual frequency range will be higher, due to resonance effects in the system.

Due to the discontinuous nature of the system, two branches of behavior exist, based on the following characteristics:

- the mass does not hit the stoppers (linear behavior)
- the mass hits (and compresses) the stoppers (nonlinear behavior)

From a frequency domain point of view, some overlap in these branches can be expected, as shown by Besselink [1] and the schematic graph in figure 2.3. This bifurcation is essential, since the main purpose of the setup is to demonstrate the existence of bifurcations and multiple solutions in nonlinear mechanical systems. For a clear demonstration, the frequency range with multiple solutions should be at least 3 Hz.

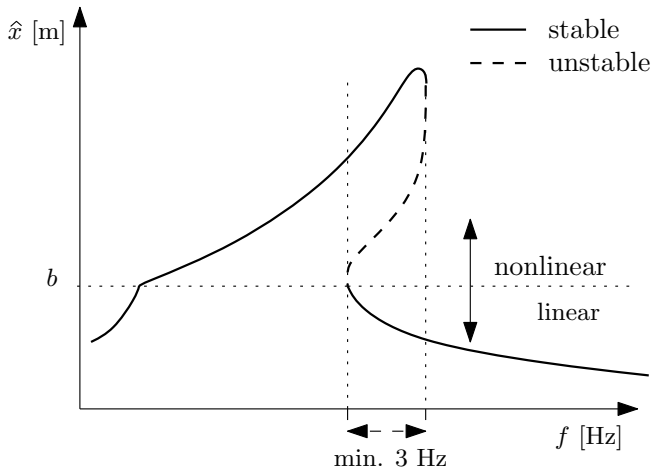

Figure 2.3: Subspaces of the SDOF system.

To summarize, it is very important that the setup serves its demonstration purposes well. This means that the dynamics of the setup must be very well observable by the audience; so the stroke of the mass ($2b$+compression of the stoppers) and the overlapping frequency-range must be as large as possible.

All concepts and decisions given in this chapter, will form a guideline for the exact design of the experimental setup in the next chapters.

Chapter 3

Numerical analysis

To obtain insight in the periodic behavior of the system presented in chapter 2, two numerical methods will be used. These are the Multiple Shooting Method and the Frequency Sweep, which will be explained in this chapter. First, the way of simulating the system will be described. Second, these two methods will be explained.

3.1 Simulation

Besselink [1] has already shown how to get a solution for systems as presented in chapter 2, by integrating equation (2.1). This can simply be done by using a standard solver, for example Matlab's ode45 solver. However, due to the different subspaces causing discontinuities, the tolerances on the time steps must be low, increasing the calculation time. To reduce this calculation time, the knowledge of analytical solutions for linear systems can be used. Within the subspaces, the dynamic behavior is linear. The discontinuous behavior is introduced on the boundaries of the subspaces, so this results in a piecewise linear system together. The behavior in the subspaces can be described in the standard form:

$$\dot{\mathbf{x}}(t) = \mathbf{A}_v(\mathbf{x}(t) - \Delta\mathbf{x}_v) + \mathbf{B}u(t) \tag{3.1}$$

Here, $\mathbf{A}_v$ denotes the system matrix in subspace v. The input matrix $\mathbf{B}$ is assumed to be equal for all subspaces, because the input u, which denotes the input force F, is a sine-function only dependent on time, thus independent on the position or velocity of the mass. The position $x = 0$ of the global coordinate system is chosen to be centered between the stoppers, so an offset has to be introduced to describe the contact regions as standard linear equations. The column Δx_v is constant and different for each subspace.

The effect of a perturbation is given by the Jacobian ($\frac{\partial \mathbf{f}}{\partial \mathbf{x}}$) of the dynamics. For linear systems, the Jacobian is simply the (constant) system matrix $\mathbf{A}$. The Jacobian also gives a differential equation for the fundamental solution matrix Φ. Since the Jacobian is constant and therefore independent of the initial conditions of the periodic solution of the system, this argument can be omitted.

$$\dot{\Phi}(t, t_0) = \mathbf{A}\Phi(t_0, t_0), \Phi(t_0, t_0) = \mathbf{I} \tag{3.2}$$

This equation is linear, so it only depends on the time span $t - t_0$. The solution of this linear differential equation is:

$$\Phi(t, t_0) = e^{\mathbf{A}(t-t_0)}\Phi(t_0, t_0) = e^{\mathbf{A}(t-t_0)} \tag{3.3}$$

The fundamental solution matrices in the linear subspaces can be calculated using equation (3.3) with the corresponding $\mathbf{A}_v$ matrix. The effect of a subspace boundary crossing on a perturbation is described by a saltation matrix. These so called saltation matrices are used to connect the linear subspaces using the transition property $\Phi(t_{si+}, t_{si-})$ (where t_{si} denotes the crossing times) resulting in the fundamental solution matrix for the entire orbit. To illustrate the use of these saltation matrices, initial condition $\mathbf{x}_0$ at t_0 is taken in subspace V_2. The mass is in subspace V_3 for $t_{s1} < t < t_{s2}$, for $t_0 < t < t_{s1}$ and $t_{s2} < t < T$ it is in subspace V_2. The end time of the movement is labeled T. The fundamental solution matrix for this orbit, separated using the transition property, is in this case:

$$\Phi(T, t_0, \mathbf{x}_0) = \Phi(T, t_{s2+})\Phi(t_{s2+}, t_{s2-})\Phi(t_{s2-}, t_{s1+})\Phi(t_{s1+}, t_{s1-})\Phi(t_{s1-}, t_0) \tag{3.4}$$

By using the definition of the saltation matrices $\mathbf{S} = \Phi(t_{p+}, t_{p-}, \mathbf{x}(t_{p-}))$ and the fundamental solution matrices for linear systems from equation (3.3), the total fundamental solution matrix is:

$$\Phi(T, t_0, \mathbf{x}_0) = e^{\mathbf{A}_2(T-t_2)}\mathbf{S}_{23}e^{\mathbf{A}_3(t_{s2}-t_{s1})}\mathbf{S}_{32}e^{\mathbf{A}_2(t_{s1}-t_0)} \tag{3.5}$$

Where $\mathbf{S}_{ij}$ denotes the saltation matrix for entering subspace i, while leaving subspace j. The saltation matrix for the SDOF model presented in equation (2.9) is given in Appendix A. For a more detailed explanation of the simulation see [1].

3.2 Multiple Shooting Method

To find periodic orbits, different methods can be used. In this report, as in [1], the multiple shooting method is used, which is a combination of the Finite Difference Method [7] and the (single) Shooting Method [7]. This method uses the Newton-Rhapson algorithm to find a zero of a multi-dimensional function. The Newton-Raphson algorithm is given in Appendix B.

An alternative is to use the (single) shooting method, which also uses the Newton-Raphson algorithm. The disadvantage of this method compared to the multiple shooting algorithm is that it uses only one shooting point. This makes it very vulnerable for obtaining convergence in case of bad initial guesses, especially in case of (very) unstable periodic solutions. The Multiple Shooting Method uses a number of points along the periodic solution, which makes it more robust. That is why the Multiple Shooting Method is used and explained in this report. For a derivation of the (single) shooting method or more details on the Multiple Shooting Method see [1] and [7].

In the Multiple Shooting Method, the N shooting points are equally spaced in time with constant time interval $h = \frac{T}{N}$. Thus $t_k = t_0 + kh$, and the N shooting points are stored in the vector $\mathbf{X} = [\mathbf{x}_1, \ldots \mathbf{x}_k, \ldots \mathbf{x}_N]^{\mathbf{T}}$. The segment connecting point $\mathbf{x}_{k-1}$ to the next point $\mathbf{x}_k$ is given by:

$$\mathbf{x}_k = \varphi_h(t_{k-1}, \mathbf{x}_{k-1}) \tag{3.6}$$

Here, $\varphi_h(t_{k-1}, \mathbf{x}_{k-1})$ denotes the solution of $\dot{\mathbf{x}}(t) = \mathbf{f}(\mathbf{x}(t), t)$ at time t_k, starting at initial condition $\mathbf{x}_{k-1}$ (at t_{k-1}). In figure 3.1 it can be seen that a solution is found if all segments are connected, so when equation (3.6) holds for all segments.

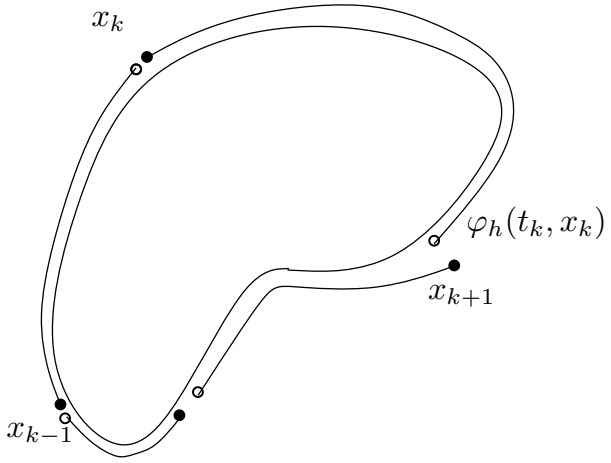

Figure 3.1: The Multiple Shooting Method.

Therefore, a periodic solution is found when a zero of the following function is found [7]:

$$\mathbf{H}(\mathbf{X}) = \begin{bmatrix} -\mathbf{x}_1 + \varphi_h(t_N, \mathbf{x}_N) \\ \vdots \\ -\mathbf{x}_k + \varphi_h(t_{k-1}, \mathbf{x}_{k-1}) \\ \vdots \\ -\mathbf{x}_N + \varphi_h(t_{N-1}, \mathbf{x}_{N-1}) \end{bmatrix} \tag{3.7}$$

Applying the Newton Raphson algorithm to find a periodic solution, gives:

$$\frac{\partial \mathbf{H}}{\partial \mathbf{X}} \Delta \mathbf{X} = -\mathbf{H}(\mathbf{X}) \tag{3.8}$$

Here, the partial derivative is given by [1]:

$$\frac{\partial \mathbf{H}}{\partial \mathbf{X}} = \begin{bmatrix} -I & 0 & \dots & 0 & \Phi_h(t_N, x_N) \\ \Phi_h(t_1, x_1) & -I & \dots & 0 & 0 \\ \vdots & \vdots & & \vdots & \vdots \\ 0 & 0 & \dots & \Phi_h(t_{N-1}, x_{N-1}) & -I \end{bmatrix} \tag{3.9}$$

In this equation, $\Phi_h(t_1, x_1)$ denotes the fundamental solution matrix at time $t_1 + h$ for a solution with initial condition x_1 at t_1. When equation (3.8) is solved (so period solution(s) are found for the system), the next iteration step can be calculated:

$$\mathbf{X}^{(i+1)} = \mathbf{X}^{(i)} + \Delta \mathbf{X}^{(i)} \tag{3.10}$$

3.3 Frequency Sweep

An alternative way of studying the (appropriate) steady-state behavior of the system is by application of a frequency sweep. This approach is often used in experiments but can also be applied numerically, although in general it asks a lot of CPU-time.

In practice a frequency sweep means applying a (slowly) increasing or decreasing frequency f to a system, this can be carried out in two manners: stepped sine or by using a constant sweep-rate. In the simulations used here, a stepped sine is used. A fixed excitation frequency is started with. This is done until a periodic solution is reached. Then the frequency f is increased or decreased with a small frequency step δf. The initial guess for this new system (with input frequency $f_{new} = f_{old} \pm \delta f$) is the state of the former derived system (with the slightly different input frequency) after an integer number of input periods. Note that the simulations have to be performed with an integer number of input periods, so that the new system can have the latest states of the former system as initial guess. In this case there is always a continuous excitation signal. Otherwise the excitation signal would have a discontinuity (when a new period is started after a non integer number of periods) and this would lead to unnecessary introduction of transient behavior. In this case there is always a smooth input function.

The advantage of this approach is that it is a relatively simple way to check whether there are discontinuous bifurcations (e.g. cyclic fold bifurcations) in a system if for one excitation signal multiple periodic solutions are found. For example when both an increasing and a decreasing frequency sweep are applied

3.4 Floquet multipliers

The stability of periodic solutions can be investigated by looking at the Floquet multipliers [9]. The Floquet multipliers are the eigenvalues of the fundamental solution matrix. When the Floquet multipliers are inside the unity circle, the periodic solution is locally stable. When they are outside the unity circle, the periodic solution is locally unstable. To illustrate this, both options are depicted in figure 3.2.

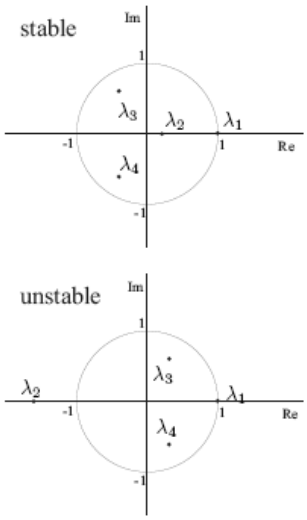

Figure 3.2: Floquet multipliers in the complex plane [7].

Chapter 4

Design of the experimental setup

The schematic system as presented in figure 2.1, can be divided into two parts: the actuator (F) and the mechanical system (m, c, k). Each of these subsystems has specific design requirements, which will be discussed next. After presenting these requirements, the exact design will be explained and visualized. All design choices are based upon the decision to keep as much system parameters variable as possible. That is, it is possible to easily adjust the mass m, spring stiffness k_i and backlash b at any time.

4.1 Means of actuation

A fundamental choice has to be made between two excitation principles:

1. excitation of the mass
2. excitation of the fixed world

Figure 2.1 is an example of the first principle: the forcing F acts upon mass m. Excitation of the fixed world could for instance be realized by a slider-crank mechanism. In this way a position will be imposed upon the fixed world. However, in order to stay as close as possible to the theories developed in [1], the mass is excited directly with a prescribed forcing. This choice also implies that a translational system will be developed, while a rotational system is a possibility too. For the translational system, the forcing actuator must fulfill some requirements:

- prescribed force independent of surroundings
- generate sinusoidal force signals up to 30 N, for frequencies ranging from 0-30 Hz
- difference between actual force output and desired output 0.2N or less than 10% of desired output
- capable of attaining high velocities and accelerations, while having a relatively low displacement (which is the case at high frequencies)
- low purchase and maintenance costs

The only commercially available actuator which meets all these requirements, is the linear motor figure 4.1. This linear motor merely consists of several permanent magnets, contained in a magnet channel, and a coil, which develops a magnetic field when a current is applied. Due to these magnetic fields, the coil and magnet channel move relative to each other.

Figure 4.1: Linear motor.

It is important to realize that the coil and magnet channel need some guidance, in order not to contact each other. To prevent the system from being subject to unknown forces, such a guidance should have the least possible dry friction. Furthermore, it should be noted that the moving part of the linear motor will be part of the total translating mass assembly m. In order to perform reproducible experiments, the initial conditions of an experiment should not change. Therefore, a spring with constant k is added to the mass. In this way it is guaranteed that the mass returns to one, unique position when at rest. The new scheme of the setup is depicted in figure 4.2.

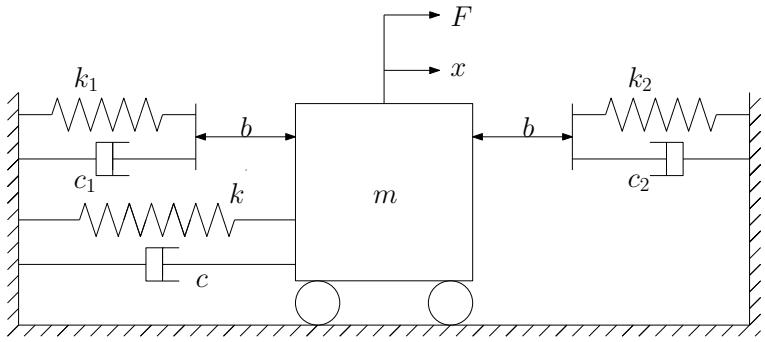

Figure 4.2: Schematic representation of the setup, including restoring spring.

4.2 Design of mechanical parts

The mass of a stopper, $m_{stopper}$, should be as low as possible. In this way, it is possible to hold the assumption from section 2.1, in which it is stated that the stopper is at rest when it is hit by the mass. Also, when $m_{stopper}$ is low, there is more freedom in choosing spring and damping constants $k_{1,2}$ and $c_{1,2}$, while the previously formulated assumption still holds. This is of great importance for tuning the overlapping frequency range.

Besides the aforementioned specific part decisions, some design decisions apply to the total experimental setup. A very important one is that, apart from the excitation, there are no electrical systems which regulate the motion of any subsystem. This means that e.g. all springs and dampers are mechanical, without any form of electrical control. The springs and dampers are assumed to have non varying spring and damping constants, within the range of operation. The values of the spring and damping constants should be realistic in the operating range of the setup, in order to be able to obtain these components easily. From for instance [2], for an amplitude larger than 5 cm, $k_{min} \geq 600$ N/m. The damper constant should be at least $c_{min} \geq 5$ Ns/m [3]. Dampers with lower damping constants (while also having a large stroke) are not very common and therefore hard to obtain.

4.3 Position measurement principles

Several measurement principles are available for doing measurements from which the position of the mass can be deduced, each with its own advantages and disadvantages. An accelerometer is a device that measures the acceleration of the mass. This signal can be integrated twice to obtain the position of the mass. A drawback is that accelerometers only measure precisely for frequencies higher than 5 Hz and they suffer drift.

Linear Variable Differential Transformer (LVDT) sensors measure positions directly, based on changes in the magnetic field of the sensor. The disadvantages of LVDT's are a limited stroke and that they add mass and friction to the moving parts of the system, on which the LVDT is partially mounted.

Because of these drawbacks, an encoder has been chosen for measuring the position of the mass. This device is very accurate (resolution up to 50 nm, analog resolution 20 μm). Measurements are being done continuously. Furthermore the encoder is capable of measuring in the desired operating range of the setup. That is, it can measure accurately in the desired frequency range (0-30 Hz) and the accompanying distance (the maximum measurable distance 70 m). The only drawback is that dust can disturb measurements. However, this drawback is small compared to the advantages. Besides the encoder, a Hall sensor is needed to control the current supply to the linear motor. A Hall sensor measures the magnetic field, from which the position dependent current input to the coil can be determined.

4.4 All parts of the experimental setup

The total design consists of the following parts:

- drive (4.4.1)
- force transducer (4.4.2)
- mass (4.4.3)
- springs (4.4.4)
- 2 stoppers (4.4.5)
- bearings (4.4.6)
- guidance bar (4.4.7)
- fixed world (4.4.8)
- damping (4.4.9)

In the next subsections each of these parts is explained in detail. When existing products are used, the serial number and most important details will be mentioned. Other details can be found in appendix D. In some subsections there will be referred to appendix C where the technical drawing can be found.

4.4.1 Drive

In the schematic layout in chapter 2, it can be seen that the mass is excited by a prescribed sinusoidal forcing F. The theory about this type of forcing is already mentioned in chapter 4, where a linear motor seemed to be means of actuation. Normally a linear motor is used to prescribe a displacement, but it is also possible, and in this case it will be used, to prescribe a force. The Anorad LEM-S-1 is the best solution, because with a magnet channel length of 300 mm the desired stroke ($2 \cdot$ amplitude) can be realized, the motor can deliver a continuous force of 26 N (peak force 83 N) and has an operating frequency which can be than 30 Hz. More details about this motor can be found in appendix E or in [5]. In figure 4.3 the magnet channel of a linear motor is presented.

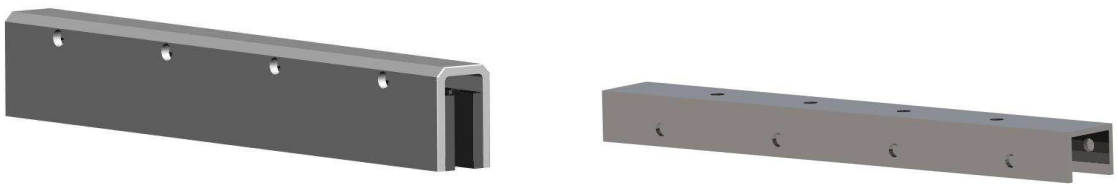

Figure 4.3: The magnet channel of the linear motor (left) and magnet channel holder (right).

Normally the coil of the linear motor is the moving part and the magnet channel is mounted to the fixed world. However, because of the wiring of the coil, the coil is mounted to the fixed world and the magnet channel moves instead. Now all the cables are fixed, otherwise the moving cables can influence the dynamical behavior. The mass must be mounted onto the magnet channel. Therefore, a magnet channel holder is designed, see figure 4.3. The mass and the magnet channel are fixed with bolts. The sum of the weights of the magnet channel, magnet channel holder, mass, tension springs and the bolts will be the total weight of the moving mass. The minimal total weight of the moving mass is 3.5 kg. A more elaborate discussion about the mass will be given in subsection 4.4.3.

4.4.2 Force transducer

In order to exert a force on the mass with the highest possible precision, this force needs to be measured and controlled continuously.

Force measurements are carried out with a piezoelectric crystal sensor (quartz plate), see figure 4.4. A Kistler 9011A has been chosen (because it is already available in the DCT-lab), which has a force measurement range up to 15000 N. More details about this sensor can be found in [4].
No power supply is needed and the deformation to generate a signal is very small. An advantage of this method is a high frequency response of the measuring system, without introducing geometrical changes to the force measuring path. This is an important advantage compared to strain gauges. The piezoelectric crystal sensor is mounted by a pre-load bolt which allows the measurement of forces in both tension and compression, see the schematic representation in figure 4.4. Closed loop measurements of the reaction force developed by the coil, make it possible to control and monitor the force delivered to the mass by the linear motor. Note that the coil of the linear motor is not mounted to the fixed world, but to the force transducer instead.

Figure 4.4: Design of the piezo sensor (left) and mounting of the sensor (right).

In figure 4.5, the assembly of the force transducer and the linear motor is presented.

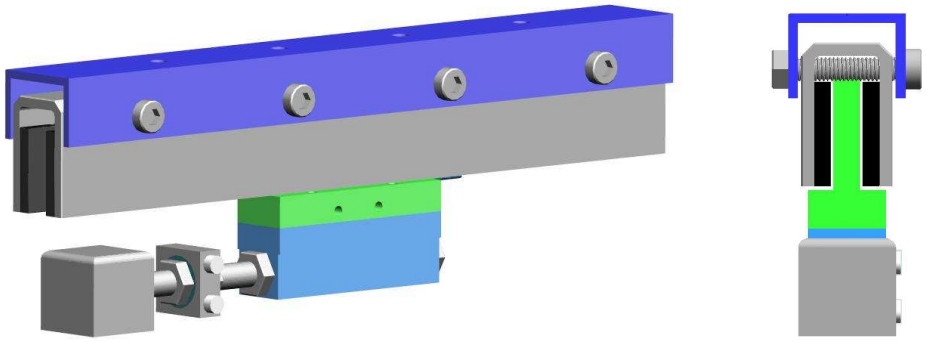

Figure 4.5: Design of the force measurement setup connected to the linear motor (3D and side view).

4.4.3 Mass

In chapter 2, it is mentioned that the prescribed force can not be very large. With a sinusoidal force amplitude of 10 N, where the derivation will be given in chapter 5, the result is a (simulated) maximal symmetrical amplitude of 23 mm. By taking twice this amplitude, 140 mm for the air bearing construction and a large margin into account, the length of the mass is 300 mm. So it will never leave the bearings at its maximal stroke.

In figure 4.6 the design of the mass is depicted and in appendix C the technical drawing of the mass is given. A triangular shape of the mass is chosen, because then the mass can be easily guided by air bearings, see subsection 4.4.6. The lengths of the sides of the triangle are set to 100 mm each, because the air bearing on each side must be in the middle and has a diameter of 50 mm.

When a high mass is vibrating at high frequencies (∼30Hz), it can become dangerous to work with due to high inertia forces. Therefore, for safety reasons, the mass is kept as low as possible. Because the mass has to be stiff and lightweight, the material chosen is aluminum. Taking into account all the demands and aspects of the system, the total weight (mass + magnet channel + magnet channel holder + bolts+ springs) equals 3.5 kg. When looking at the triangular mass with a total length of 300 mm and sides of 100 mm, it is clear that this will be much heavier than 3.5 kg. Therefore the weight of the mass needs to be reduced. This is done by making a lacing construction, so material will be removed to lower the weight. The only demand for this lacing construction is that there must be a hole in the mass where the guidance bar can be put through (see subsection 4.4.7).

The last design aspect of the mass are the drilled holes with threat in the three corners of the triangular cross-section, which are chamfered to reduce weight. The holes on the bottom are for attaching the linear motor. In the holes on the other two chamfered corners other bolts can be put to increase the weight in additional experiments. In figure 4.6, it must be mentioned that the lacing construction is not included in the design, because the exact form will be determined by the manufacturer, who has the skills to make a good design. Ulti-

mately, due to the lacing construction, the triangular mass will have a weight of 1 kg without the additional bolts. Together with 1.7 kg for the magnet channel which is attached to the triangular mass, 0.3 kg for the magnet channel holder and 0.5 kg for the four tension springs, the total minimal moving mass is 3.5 kg.

Figure 4.6: Design of the triangular mass.

In figure (4.7), the total moving mass is shown. As mentioned before, it consists of four extension springs, the magnet channel and its holder and the triangular mass. When the triangular mass hits the stoppers, the mass of the moving part is increased by the mass of the stoppers.

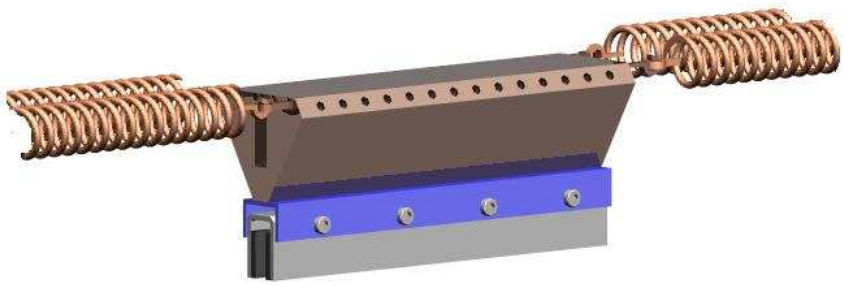

Figure 4.7: The moving part in the complete setup.

4.4.4 Springs

Two types of springs are involved in the design, i.e. compression and extension springs. The spring in the stopper is a compression spring and will be mentioned together with the design of the two stoppers in subsection 4.4.5. The mass is connected to the fixed world by two pre-stressed extension springs on each side. Each spring is pre-stressed with the maximal amplitude of the mass, which is 23 mm according to subsection 4.4.3. The extension spring is depicted in figure 4.8. The aim of these springs is to give the mass an initial position in the middle and they will contribute to the dynamical behavior. For these springs some calculations are made. The maximum extension of one spring is the same as twice (due to pre-tensioning) the amplitude of the mass. The spring constant is not constant if the spring is too short compared to the maximum extension. The extension springs are chosen from [2], having serial number T32240, a total length of 290 mm, a nominal length of 175 mm and an estimated mass of 0.102 kg. The nominal length is now at least twice the maximal amplitude of 23 mm of the moving mass. Within this nominal length the force-extension behavior is linear according to [2]. Details on the stiffness and eigenfrequency will be given in chapter 5.

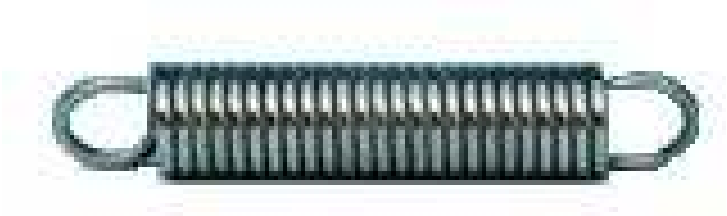

Figure 4.8: The extension spring.

4.4.5 Stoppers

In figure 4.9 the design of the stopper is depicted. The stopper consists of a compression spring which is connected to the fixed world and is also visualized in figure (4.9). The compression spring is supplied by [2] with serial number D14110 and has a length of 195 mm. A guidance is designed, so the mass will push against a stiff construction instead of a hanging spring. The base of the stopper is therefore a roll bearing which slides on a guidance bar (see subsection 4.4.7). Chosen is a roll bearing from SKF, serial number LBBR 8. It is very small with respect to the mass. Therefore, a round metal plate is fixed on it, with the technical drawing given in appendix D. This round metal plate has a large diameter, so it collides with a large area of the moving mass. The stopper plate is connected to a spring, which is attached to a nut (left part in figure 4.9), which can be screwed onto the guidance bar. The mass of both stoppers is part of the total mass of the moving mass in the contact mode. The stopper should be kept as low as possible as mentioned earlier. Therefore the round plate is made of aluminum. To reduce the weight, holes have been made in the stopper plate, so the total estimated moving mass is 0.140 kg (the total weight of the stopper plate and spring is 0.390 kg, but due to limited compression of the spring, 0.140 kg is a safe estimate). The guidance bar in figure (4.9) is not a part of the stopper, but it gives a better presentation of a part from the final design.

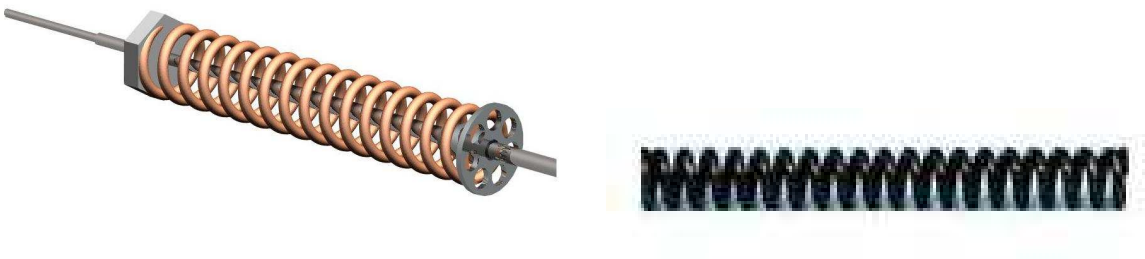

Figure 4.9: Design of the stopper (left) and the compression spring (right).

4.4.6 Air bearings

The magnet channel, with the mass mounted on it, can move along the coil. To avoid friction, there must be a gap between the magnet channel and the coil. Therefore, the mass must be supported. This is done using air bearings. Figure 4.10 shows the air bearing which will be used in the construction. The general advantage of air bearings is that they have very low friction. With an air bearing on each side of the triangular mass, all degrees of freedom, except for the direction of the linear motor's length axis, are fixed. Air bearings from Fabreeka are used, similar to the ones used in the experimental setup of Niels Mallon at the TU/e. The minimal air pressure is 2 bar and can be increased to 7 bar. The maximal bearing load is 339 kg.

Figure 4.10: Design of the bearing (left) and bearing holder (right).

The air bearings have to be attached to the fixed world. Therefore triangular shaped frames are designed. This is a schematic design, because there must be made a trade-off between visibility and stiffness. In figure 4.10 the construction is given (including the air bearings). In each bearing holder a set of three air bearings with a diameter of 50 mm each is used.

When the air bearings are mounted on these frames, a gap of 10 μm is left between the mass and the bearing. In this gap air pressure can rise. When placing only one set of air bearings in the middle of the mass, the mass will tilt, using two sets of air bearings will avoid that. The position of the air bearing holders is 100 mm from the ends of the mass. Because then the mass will never leave a bearing at its maximum stroke. To adjust height, blocks can be placed under the air bearing holders, as can be seen in figure 4.11, where the assembly of the air bearings and holder is presented. The dimensions of the bearing holder are given in appendix C.

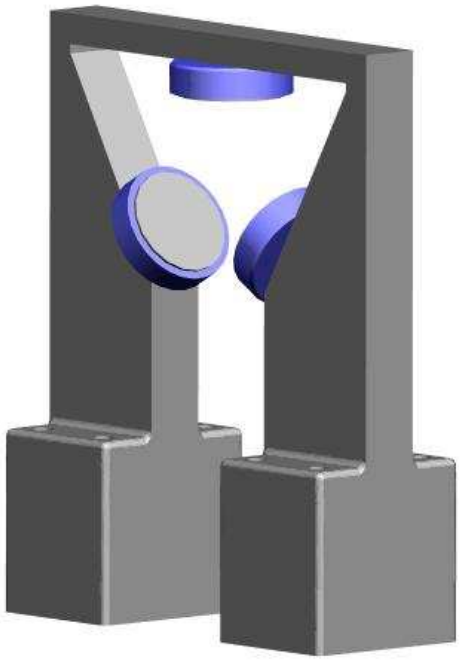

Figure 4.11: Assembly of the air bearings.

4.4.7 Guidance bar

The guidance bar is used to guide the stoppers. The design of the guidance bar is given in figure 4.12 and the technical drawing can be found in appendix C. The length of the guidance bar is determined by the length of the mass, the backlash between the stopper and the mass and the length of the extension springs on each side. The total length is 1270 mm, this is also approximately the total length of the setup. A threaded bar makes it possible to adjust the backlash, i.e. the distance between the stopper plate and the mass, by moving the nut of the stopper. There are two stoppers and therefore the above mentioned details are symmetrical. The bar is at both threaded ends connected to the fixed world by nuts. In this way the guidance bar is pre-tensioned and it will not vibrate due to its length, gravity or disturbing forces that are acting on it.

Figure 4.12: Design of the symmetric part of the guidance bar

4.4.8 Fixed world

Some of the earlier mentioned parts must be connected to the fixed world. Due to the design and the position of these parts, the choice has been made to give the fixed world the shape of a large letter U as can be seen in figure 4.13. A trade-off between a low mass and a high stiffness is made. An aluminum bottom plate with aluminum sides at both ends are used to keep the weight as low as possible. An aluminum plate at the back is fixed to the bottom plate and both sides to make the construction more stiff. The technical drawing can be found in appendix C. The total length of the experimental setup is about 1260 mm. The aluminum sides are connected to the bottom plate with bolts as can be seen in figure 4.13. The height of these sides, which is also the total height of the setup, is 250 mm. The dimensions are in such a manner that it is portable, a demand in the design process. The thickness of the aluminum bottom plate, is chosen to be 10 mm, for a high stiffness while still being relatively light-weight. The thickness of the sides is chosen to be 20 mm, for the same reason as mentioned for the bottom plate. The total experimental setup will have a weight of about 30 kg.

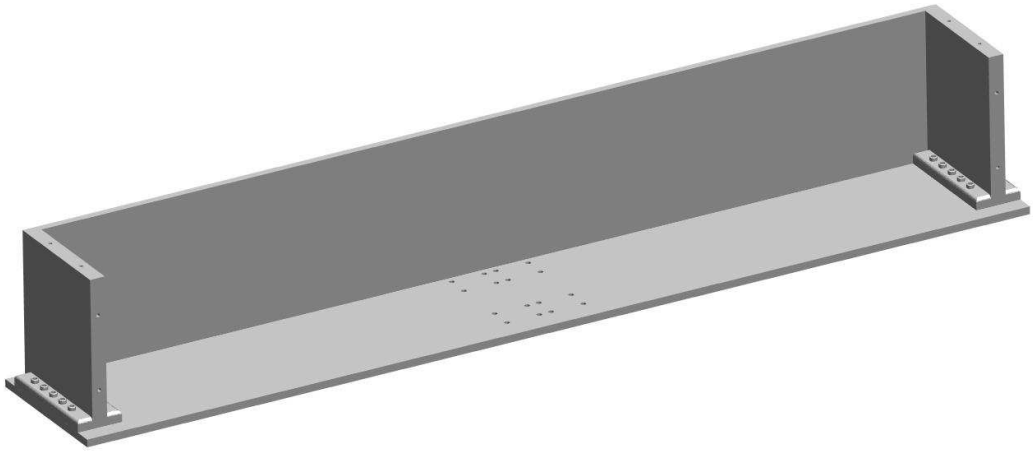

Figure 4.13: Design of the fixed world.

4.4.9 Damping

The last remark on the experimental setup is the removal of the dampers. In the schematic representation from the system in section 4.1, dampers are included. During the design process it was tried to include these dampers in the final setup. However, there are no commercially available dampers with the demanded stroke and damping constant. On the contrary, there

will always be little damping present in the setup, for example material damping, friction in the air bearings and stopper bearings and damping in the non elastic collision of the mass with the stoppers. These damping values are not known yet.

4.5 Complete experimental setup

In figure 4.14 the total assembly is presented. A transparant plastic guard is mounted on the vertical sides of the fixed world. This guard covers the entire setup and protects both the operator as well as the setup. The technical drawing of this safety cover is given in appendix C.

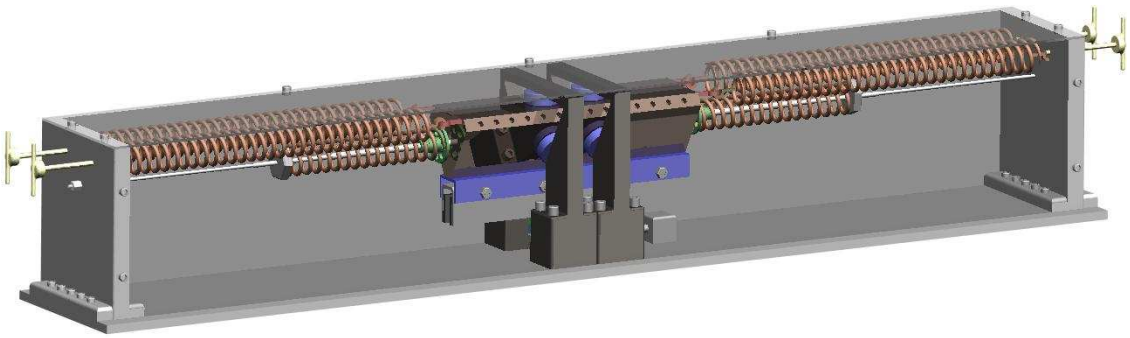

Figure 4.14: Design of the complete experimental setup.

Chapter 5

Simulation results

In chapter 2, the mathematical model for the system studied in this report has been given. To find periodic solutions for this model, chapter 3 dealt with the numerical part and presented two methods to solve the equations: the Multiple Shooting Method and the stepped Frequency Sweep approach. In this chapter, this theory will be used to obtain solutions for the system, with the parameters corresponding to the choices made in the previous chapter.

5.1 Parameters

With the design choices made in the previous chapter, the following parameters are found for the numerical model:

Table 5.1: Systems parameters

Parameter	**Value [unit]**
A	10 [N]
m	3.5 [kg]
b	0.01 [m]
k	$2.72 * 10^3$ [N/m]
c	3.892 [Ns/m]
$m_{stopper1}$	0.14 [kg]
k_1	$2.01 * 10^4$ [N/m]
c_1	7.6364 [Ns/m]
$m_{stopper2}$	0.14 [kg]
k_2	$2.01 * 10^4$ [N/m]
c_2	7.6364 [Ns/m]

In table 5.1 it can be seen that stopper 1 and 2 have the same parameters, so the two stoppers are identical. The peak force applied, in other words the amplitude of the sine excitation applied to the system, is 10 N. The mass m is the total mass of the moving part, as explained in chapter 4. This includes the triangular mass, the magnet channel, the connecting parts and a part of the total mass of the springs (30%[1]) of $4 * 0.102kg$. The masses of the stoppers $m_{stopperi}$, are the sum of the masses of the moving parts of the stoppers, which are the plate, the roll bearing and a part of the spring (which is about 30 % of the mass of the spring

(0.38 kg) [1]). The stiffness applied to the mass k can be found by summing the stiffnesses of the four identical springs attached to the mass. The damping constants c and c_i are derived by introducing a small amount of (modal) damping namely 2% ($\zeta = 0.02$). With this given dimensionless damping ratio ζ, the damping constants c and c_i are derived by [8]:

$$c = 2\zeta m\omega_n \tag{5.1}$$

Equation (5.1) is only suitable for linear systems. The real damping of the system is not known yet, but obviously there is always some damping in a mechanical system, as mentioned before in subsection 4.4.9. This is not the only reason for introducing this little damping, it also improves and speeds up the numerical convergence process to find periodic solutions. The mass m is derived by selecting the lowest mass possible, which is 3.5 kg. This is the standard mass when no mass is added to the triangular part.

5.1.1 Results Multiple Shooting Method

With the parameters given in table 5.1, the Multiple Shooting Method from chapter 3 is used to study the system. The result is given in figure 5.1. The blue lines are the periodic solutions found by applying the shooting method. The green lines are estimated periodic solutions based on an earlier study [6]. Here a solid line is a stable periodic solution, while a dashed line is an unstable periodic solution. These periodic solutions are not found in the simulations, due to problems with the convergence of the numerical process to a periodic solution, the tolerances concerning the convergence can not be met.

In this figure the input frequency is given on the horizontal axis and the vertical axis represents the maximum absolute excitation from the original position $x = 0$. For the input frequency range between about 5 and 9 Hz two stable periodic solutions are possible. This implies that there is nonlinear behavior in the system. To get some insight in the stability of these solutions found, the (two) Floquet multipliers are derived. These are plotted in figure 5.2. The values of these Floquet multipliers are all below 1, so the periodic solutions found are stable.

5.1.2 Results Frequency Sweep

The same system as in the previous section is studied, but this time the stepped Frequency Sweep method from chapter 3 is used to investigate the system. The frequency steps δf used, are 0.01 Hz between the frequencies 0.2 and 6 Hz, from 6 to 20 Hz a step size of 0.1 Hz is taken. The result is given in figure 5.3. Here the same nonlinear behavior is found as in the Multiple Shooting Method, depicted in figure 5.1. These two results show about the same behavior as the system studied in [6]. In the results found here, there is no contact with the stoppers for amplitudes smaller than b (0.01 m). In case the stoppers would have been absent, the response curve would show a linear harmonic resonance peak at the eigenfrequency equal to 4.4 Hz ($\omega_n = \sqrt{\frac{k}{m}} = 27.9\ [rad/s]$). In this case, for amplitudes higher than b m, there is contact with the stoppers.

[1] Note: 30% of the mass of the total springs is taken, probably this is a high estimate, because the mass only moves maximally 0.023 m, while the length of the springs is over 0.1 m, so 30% is a large margin (it is taken so large to be sure that the mass of the springs is not taken to low)

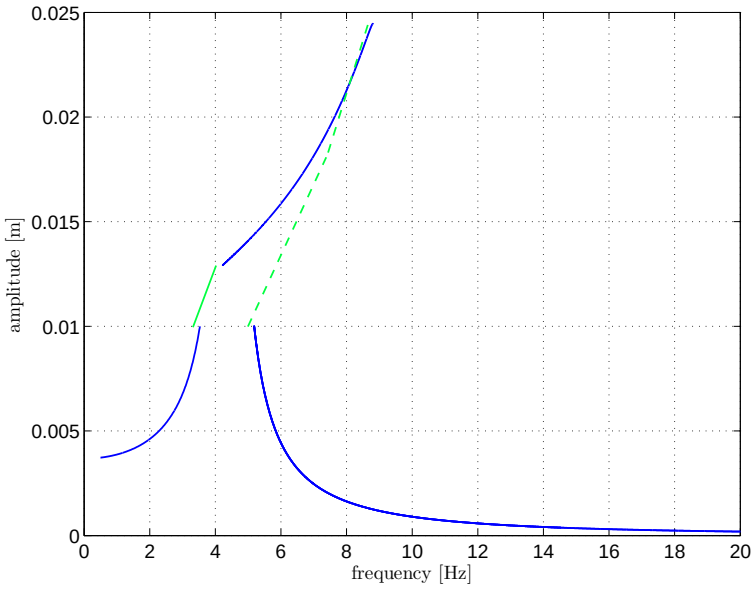

Figure 5.1: Response diagram found with the Multiple Shooting Method.

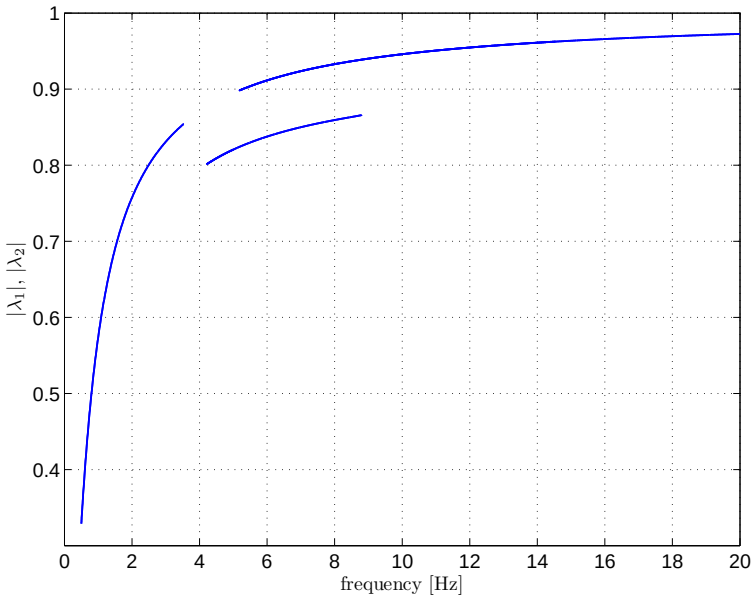

Figure 5.2: Floquet multipliers.

Summarizing, the simulations show that the experimental setup does exhibit nonlinear behavior (to be specific: piecewise linear behavior). The frequency range in which two stable solutions exist, is more than 4 Hz (from 5 to 9 Hz). In this range, the two branches of periodic solutions show a big differences in amplitude (a minimum of 5 mm vs. 23 mm at maximum). The damping constants taken in the simulation are based on the assumption of 2 % damping. In reality, it is likely that this percentage is lower, causing higher amplitudes than 23

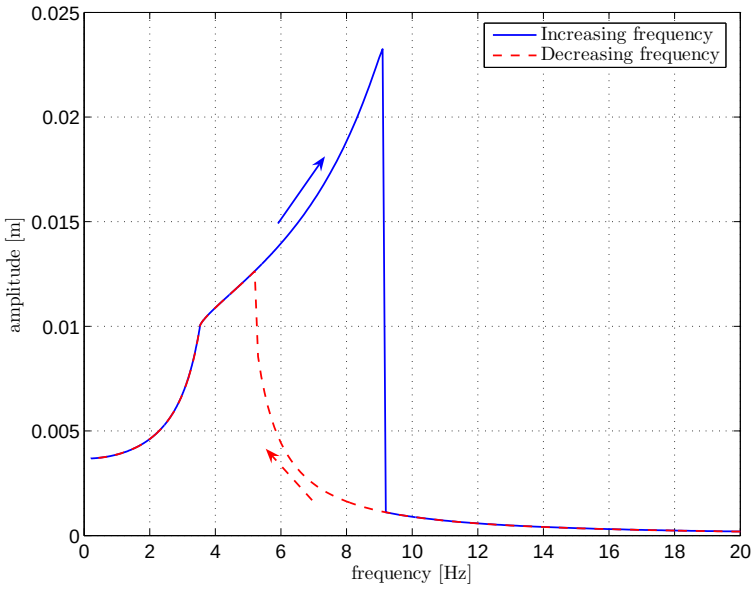

Figure 5.3: Response diagram found with the Frequency Sweep.

mm. The demand of 50 mm backlash on both sides from chapter 2 has appeared to be not feasible, because excessive forces and strokes would occur. This means that the visibility of the movement is not as high as demanded, but due to the stopper compression and audible effects, it is expected that the nonlinear behavior can be observed still very well. All this means that in reality a bifurcation with at least 4 Hz overlap certainly will be observed. The magnitude of the amplitude in practise will depend on the amount of dissipation, which is still unknown. Therefore the experimental outcome is not perfectly predictable. The mass of the total setup will be approximately 30 kg, so the demand of the maximal mass not higher than 30 kg (as presented in chapter 2) is met. Due to the pretensioned springs attached to the mass, the length of the setup is 1260 mm. This means that the original design requirement (maximal length is 1000 mm) is exceeded with 260 mm. This length could be decreased by choosing other springs, while have the same stiffness. However, for experimental flexibility, the dimensions are chosen very high. In this way, many (linear) stiffnesses and amplitudes can be experimented with. Different springs can be designed and be made by hand, but in this report only the commercially available springs are studied. The formula for the stiffness of a spring is [10]:

$$k = 1000\frac{Gd^4}{8D^3n}; \tag{5.2}$$

Where G denotes the shear modulus, d the diameter of the wire, D the diameter of the spring and n the number of windings of the spring.

Both numerical approaches found about the same periodic solutions. But they do differ very much in calculation time. The Multiple Shooting Method uses about a quarter of an hour, while the Frequency Sweep uses about three hours of CPU-time[2].

[2]In this study an Intel(R) Pentium(R) M 1400MHz processor is used

Chapter 6

Fixed world excitation

During the design of the experimental setup, an alternative type of excitation (prescribed displacement) has been considered. The reason for this was the uncertainty of controlled force excitation of the linear motor in the final design. Although this seems possible after all, this still needs to be worked out into detail. The alternative, the fixed world excitation, is discussed in this chapter. Many of the previously designed parts can also be used in this alternative. This includes the (expensive) linear motor. To understand the principle of the fixed world excitation, the idea is presented in figure 6.1.

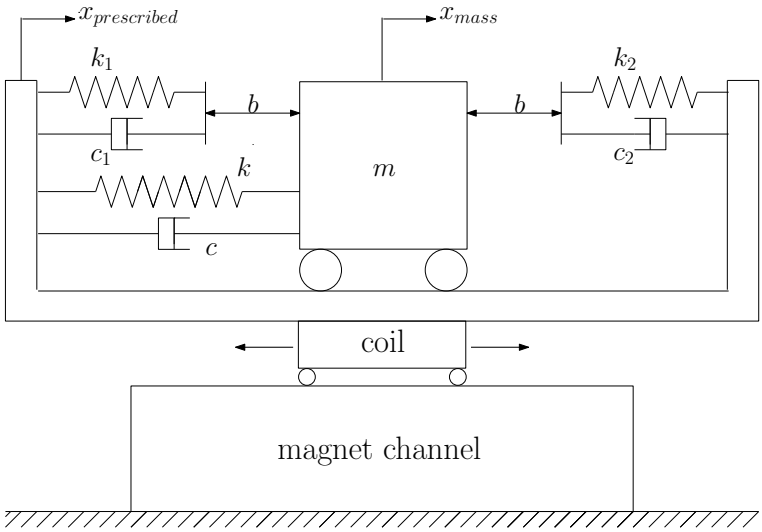

Figure 6.1: Fixed world excitation

6.1 Explanation of the fixed world excitation

The concept of the final design, as presented in the previous chapter, is used. The alternative idea is that the fixed world is connected to the coil and can be moved by the linear motor, which is mounted on a table for instance. The mass is guided on the fixed world and does not move if the coil is not moving. It is not easy to use air bearings for the guidance of the mass this time. Now a single guidance rail, which is connected to the fixed world, is used above

the mass. A moving block on this rail is connected to the mass. There is no danger that the mass is going to set, because there is used one rail only. The benefit of this guidance rail is lower the price compared to the air bearings. The original guidance bar can still be used to guide the stoppers. The weight of the fixed world is quite high. This can lead to a high force amplitude in case of excitation at high frequencies. Therefore the fixed world should have the lowest possible mass, keeping in mind that it must remain stiff. Summarizing: most parts from the mass excitation design can be used for the fixed world excitation as well:

- Drive
- Mass
- Stopper
- Guidance bar
- Springs

So it is possible to change the design if necessary, without high additional costs.

Chapter 7

Conclusions and Recommendations

7.1 Conclusions

In this report, the design and construction of an experimental setup of an SDOF system with backlash has been discussed. Such an experimental setup can serve to get more insight in the dynamic behavior of commonly used real life systems with backlash, like gear systems. Moreover, it can be used to verify theoretical models with. The designed experimental setup mainly consists of a resiliently mounted mass, that can move between two stopper springs, which are mounted on both sides of the mass. Between the mass and each stopper, backlash is present. Furthermore, in the proposed design, the mass is periodically excited by a sinusoidal force, generated by a feedback controlled linear motor. The controller is to be designed.

The design meets various design constraints, like e.g. a low, sinusoidal excitation force (max 10 N), a bifurcation range of 4 Hz and adjustable parameters (b, k_i, m). The design process has been carried out by means of numerical simulation, with various sets of parameters. Special attention has been payed to safety and demonstration purposes of the setup. That is, the magnitudes of the forces that occur in the setup do not pose a direct safety hazard.

Also, the dimensions and weight of the experimental setup are such that it can perfectly well serve as a demonstration model; both in the sense of portability of the complete setup itself, as well as the observability of the dynamics of the setup. Furthermore, an alternative way of excitation has been proposed. In this proposal, the fixed world is excited instead of the mass. Even though these two ways of excitation are very different, the most expensive parts of these setups are the same. In this way costs can be kept as low as possible. For a list of the construction costs, see appendix E. Due to a lack of time and financial resources, the experimental setup has not been built yet.

7.2 Recommendations

For future work, the following recommendations are given:

- Build the experimental setup. The design of the air bearing holder should be improved, however. The current design is not as stiff as possible, but it does indicate the size of such an air bearing holder.

- Design the feedback controller for the periodic force excitation.
- Do preliminary dedicated collision experiments between mass and stopper to estimate damping levels.

The latter two of the aforementioned recommendations, can be carried out only when the physical (sub)systems of the experimental setup are available.

- Experiment with the experimental setup, in order to validate the theory.
- Experiment with different sets of springs, variable mass and backlash parameters. Special attention has been paid in the design to make this possible.

Bibliography

[1] B. Besselink. *Periodic orbits in systems with backlash: stability, classification observability.* Eindhoven University of Technology, 2007.

[2] Catalogue Tevema Technical Supply B.V.Amsterdam.

[3] http://www.airpot.com/beta/html/exhibit30.html.

[4] http://www.kistler.com/do.productfinder.nl.nl nl?content=13_Productfinder&param=App.9011A.5.

[5] http://www.rockwellautomation.com/anorad/products/linearmotors/epoxycore/lem.html.

[6] R.I. Leine and D.H van Campen. *Discontinuous fold bifurcations in mechanical systems.* Eindhoven University of Technology, 2002.

[7] R.I. Leine and N. van de Wouw. *Numerical Methods for Computing Periodic Solutions*, 2005.

[8] J.L. Meriam and L.G. Kraige. *Engineering Mechanics: Dynamics.* John Wiley and Sons, Santa Barbara, fourth edition, 1998.

[9] J.J. Thomsen. *Vibrations and Stability: advanced theory, analysis, and tools.* Springer, Berlin, 2nd edition, 2003.

[10] Luhn und Pulvermacher. *Stahlfedern: Berechnung und Gestaltung.* Baldur, Hagen-Haspe, 1980.

Appendix A

Saltation matrix

The saltation matrices S_{ij} (describing the change in a perturbation when crossing the boundary between subspaces V_i and V_j) is found by using definition:

$$\mathbf{S} = \mathbf{I} + \frac{(\mathbf{f}_{p+} - \mathbf{f}_{p-})\mathbf{n}^T}{\mathbf{n}^T \mathbf{f}_{p-}} \tag{A.1}$$

Here, $\mathbf{n}$ is the normal which is defined as $\mathbf{n}(\mathbf{x}) = \nabla h(\mathbf{x})$. Where the property $h(\mathbf{x}(t_p)) = 0$ is used. Where t_p is the crossing time. Furthermore the $\mathbf{f}_{p+}$ and $\mathbf{f}_{p-}$ are calculated as follows:

$$\mathbf{f}_{p+} = \mathbf{f}(t_{p+}, x(t_{p+})) \tag{A.2}$$

$$\mathbf{f}_{p-} = \mathbf{f}(t_{p-}, x(t_{p-})) \tag{A.3}$$

This results in the following saltation matrices:

$$\mathbf{S}_{12} = \begin{bmatrix} 1 & 0 \\ -\frac{c_1}{m} & 1 \end{bmatrix} \tag{A.4}$$

$$\mathbf{S}_{21} = \mathbf{I} \tag{A.5}$$

$$\mathbf{S}_{23} = \mathbf{I} \tag{A.6}$$

$$\mathbf{S}_{32} = \begin{bmatrix} 1 & 0 \\ -\frac{c_2}{m} & 1 \end{bmatrix} \tag{A.7}$$

The saltation matrices show that the fundamental solution matrix only jumps when contact with a stopper is engaged. This is due to the damping force in the stoppers, which gives a discontinuity in the total force on the mass. Since contact with the stoppers is lost when the contact force is zero, leaving a stopper does not result in a jump in the fundamental solution matrix [1].

Appendix B

Newton-Raphson algorithm

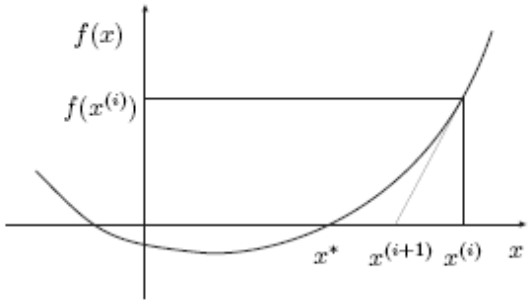

Figure B.1: The Newton-Raphson algorithm

As is stated in [7], the Newton-Raphson method finds a zero point x^* of a function $f(x)$. In figure B.1 a nonlinear scalar function $f(x)$ with a zero point at x^* is shown. To find this zero point, an initial guess $x^{(0)}$ is needed and iteratively a zero can be found. The Newton-Raphson algorithm uses the local tangent $f'(x)$ of the function f(x). Let $x^(i)$ be the result of the previous iterate of the Newton-Raphson process. The next iterate $x^(i+1)$ is then found by extrapolation of the local tangent $f'(x^{(i)})$ towards the x-axis (see Figure B.1):

$$x^{(i+1)} = x^{(i)} - \frac{f(x^{(i)})}{f'(x^{(i)})} \tag{B.1}$$

The Newton-Raphson algorithm does not converge for all functions or might converge to another zero of the function. The initial guess should be close enough to obtain convergence for an arbitrary function $f(x)$. It might also be that the iterative process converges to another zero of the function. The equation (B.1) is iteratively used until some convergence criterion is met or is stopped when the method diverges. Most convergence criteria let the algorithm stop when the value of $f(x(i))$ lies within some tolerance from zero. The scheme is usually halted when the scheme is not converging monotonically, $f(x(i+1)) > f(x(i))$, or when a maximum number of iterations is exceeded. The NewtonRaphson algorithm can also be applied to find a zero of a multi-dimensional function $\mathbf{f}(\mathbf{x})$. One then has to solve in each iteration step the following set of linear equations:

$$\mathbf{Df}(\mathbf{x}^{(i)})\Delta\mathbf{x} = -\mathbf{f}(\mathbf{x}^{(i)}) \tag{B.2}$$

to obtain the update $\Delta\mathbf{x} = \mathbf{x}^{(i+1)} - \mathbf{x}^{(i)}$. The NewtonRaphson algorithm is a gradient method because it uses the gradient $\mathbf{Df}$ (being the Jacobian matrix). The calculation of $\mathbf{Df}$ might be numerically expensive, which is a drawback of the NewtonRaphson method and of gradient methods in general. The merit of gradient methods is a relatively good convergence rate.

Appendix C

Technical drawings

All drawings and sizes are given in this appendix.

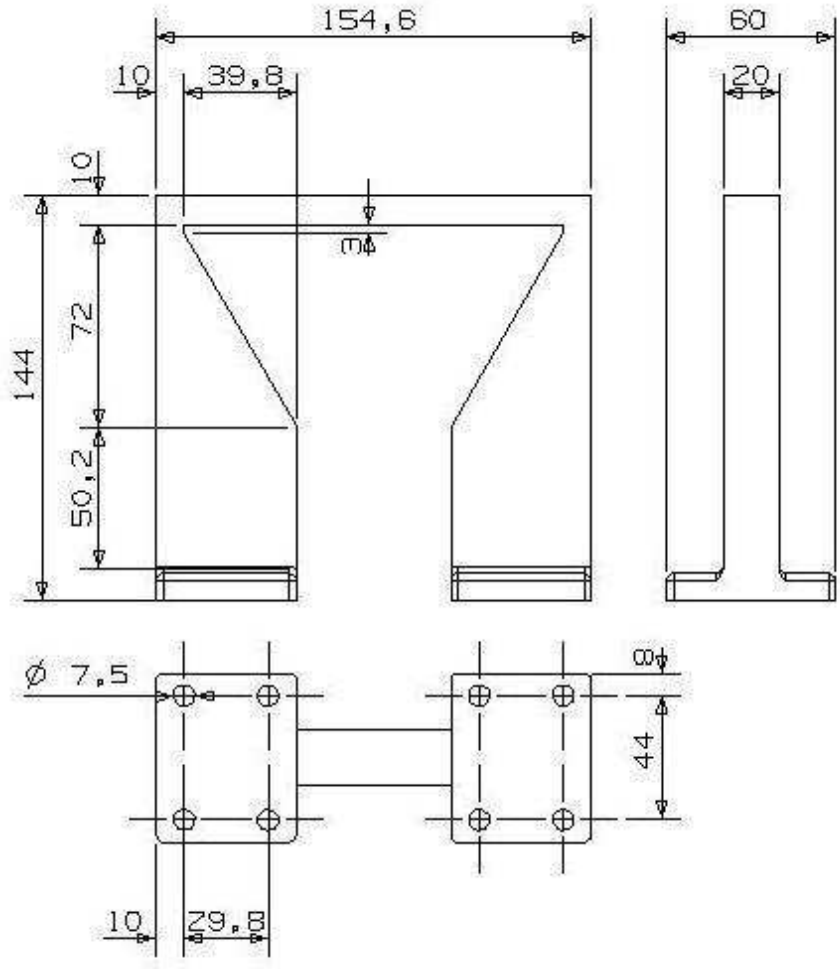

Figure C.1: A Schematic design of the air bearing holder where the dimensions are only a global indication of the final design.

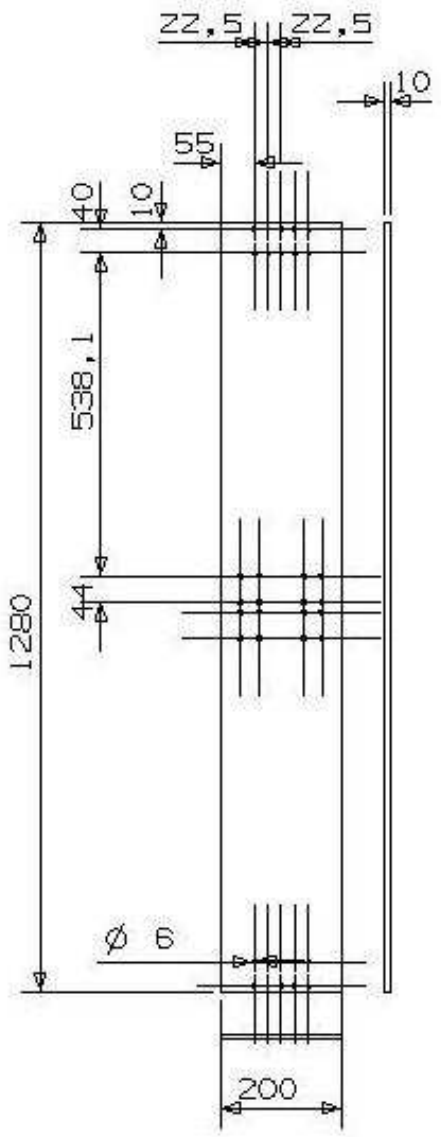

Figure C.2: Technical drawing of the bottom plate.

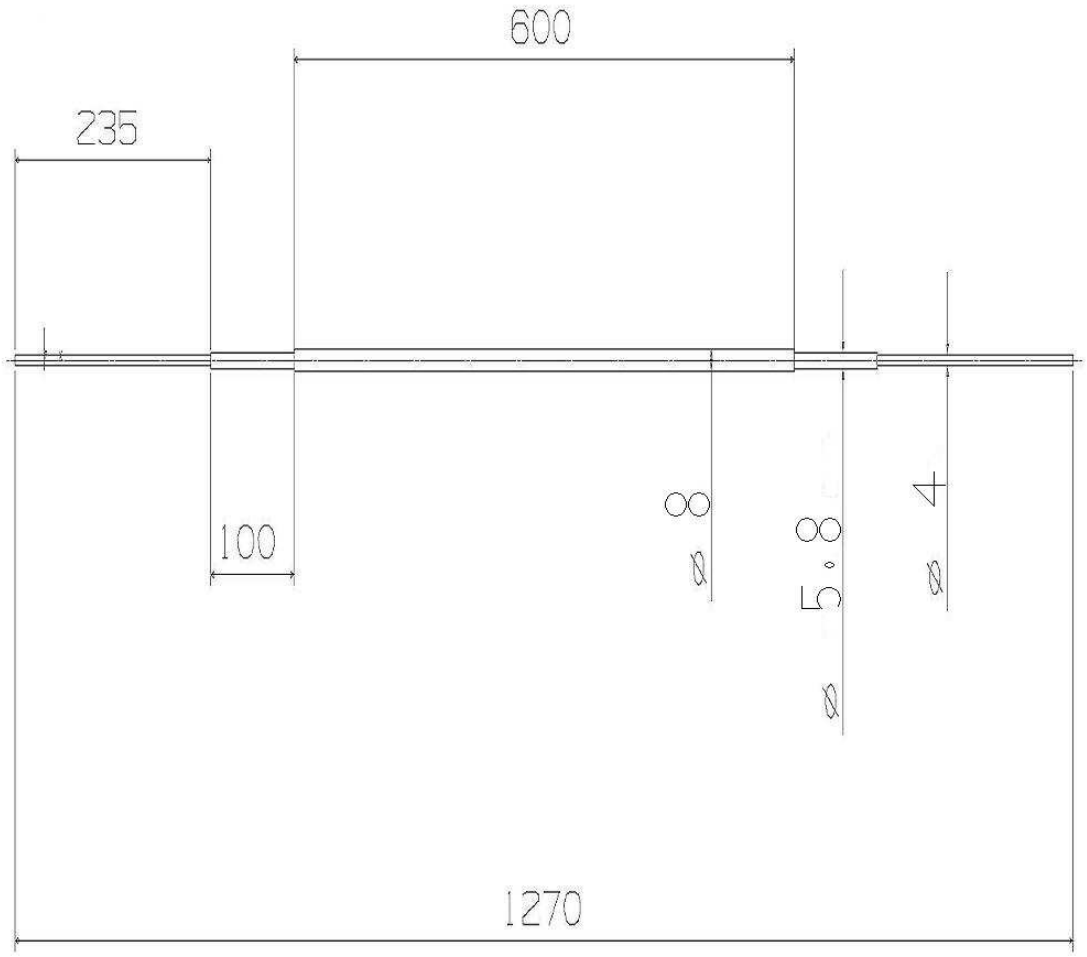

Figure C.3: Technical drawing of the guidance bar.

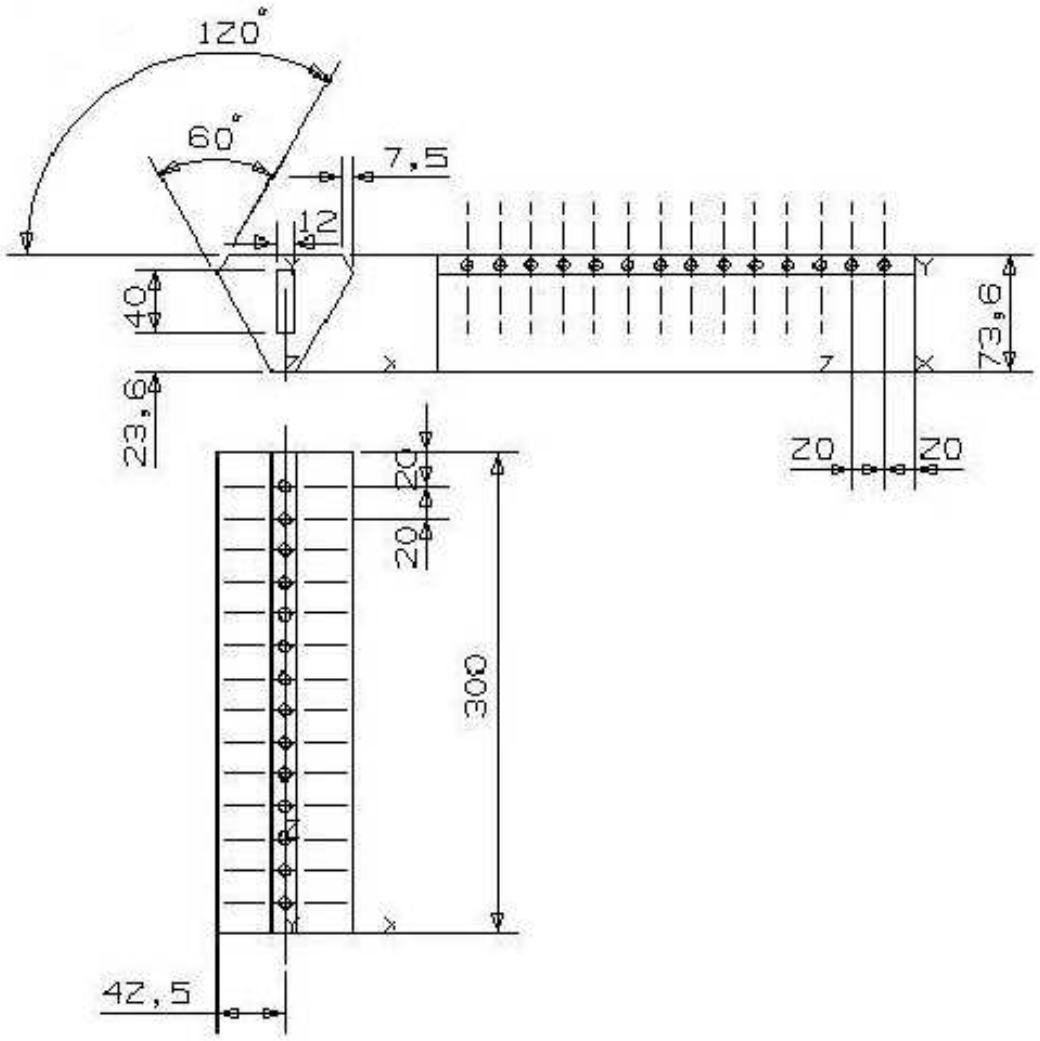

Figure C.4: Technical drawing of the mass.

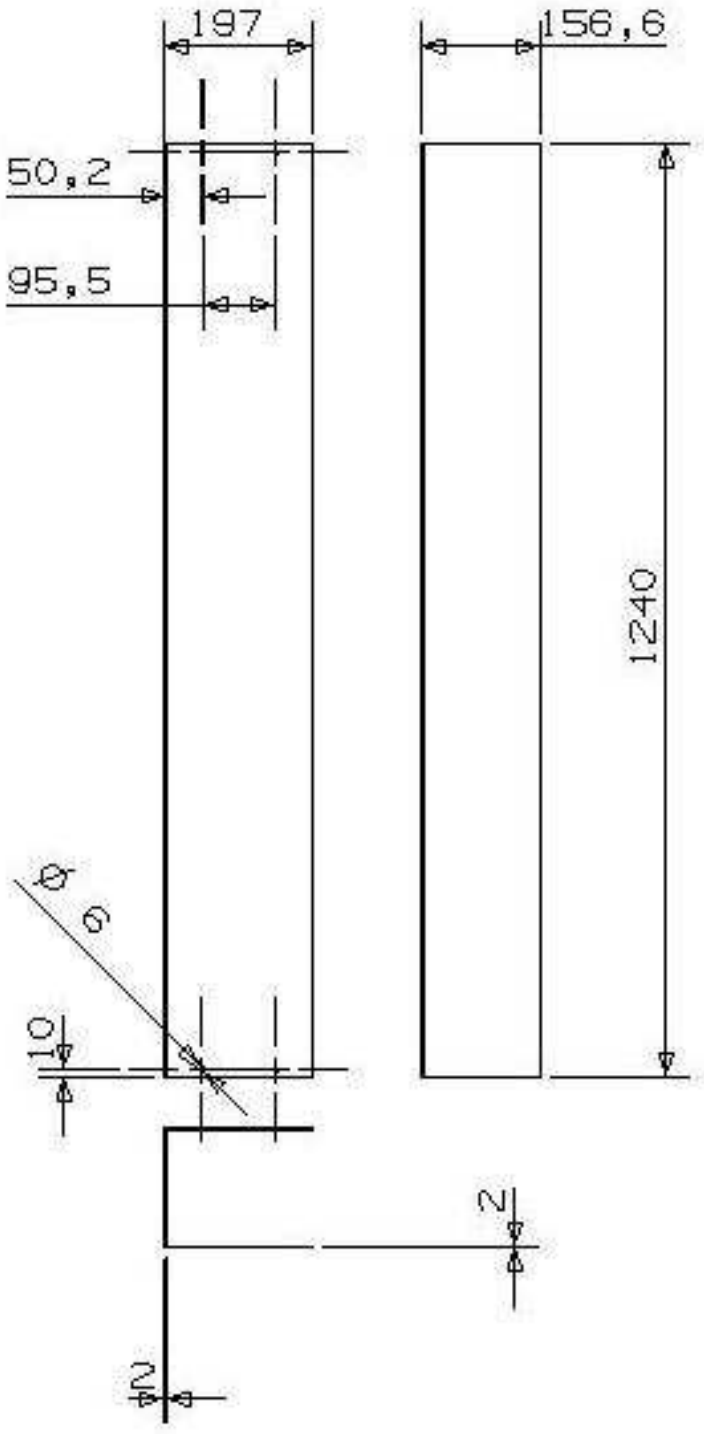

Figure C.5: Technical drawing of the protection cover.

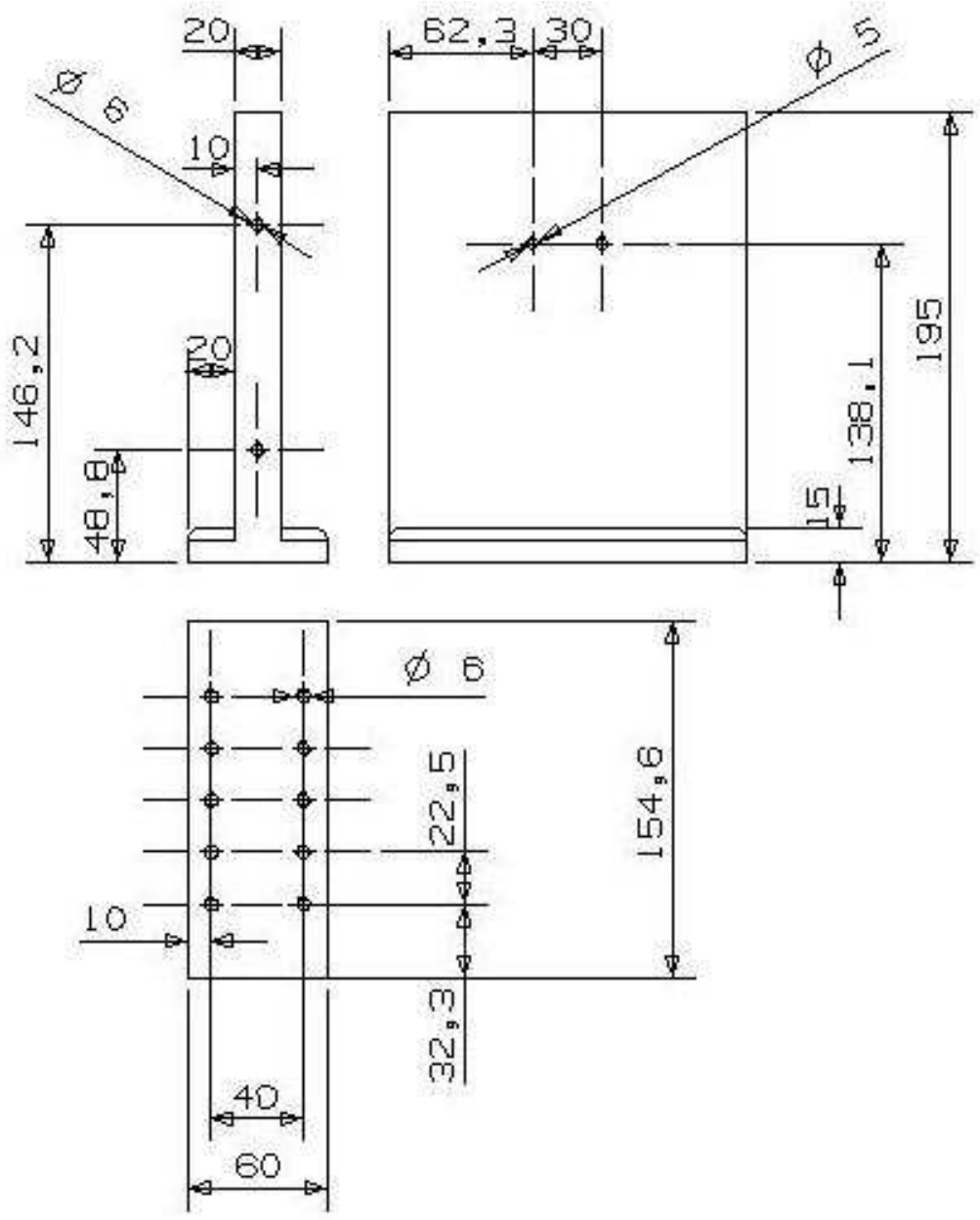

Figure C.6: Technical drawing of the side plate.

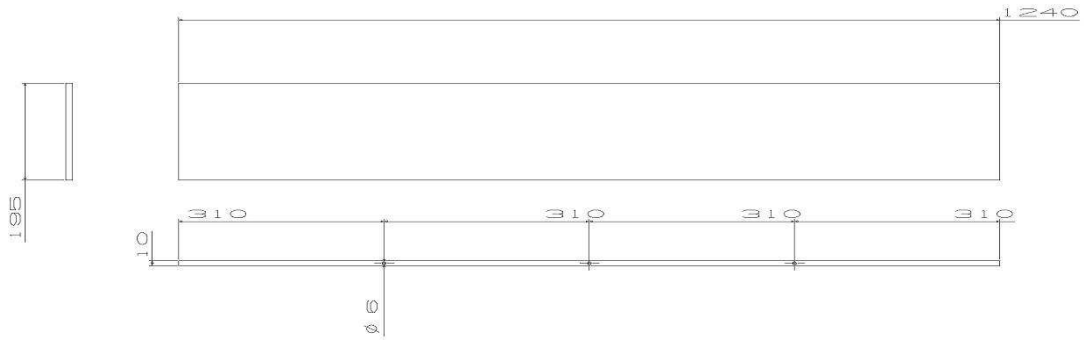

Figure C.7: Technical drawing of the back plate.

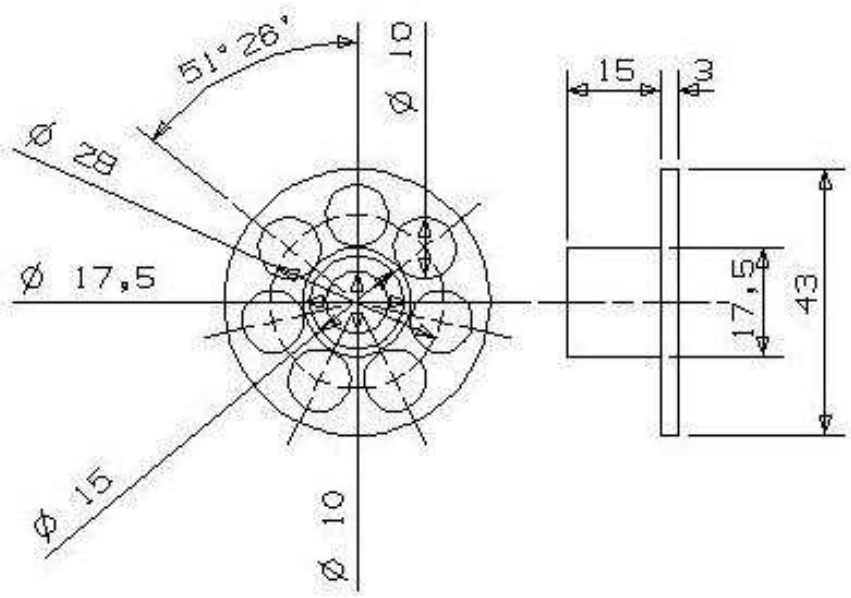

Figure C.8: Technical drawing of the stopper plate.

Appendix D

Parts List

All existing parts with their known details are given in this appendix.

D.1 Piezo crystal sensor

Manufacturer: Kistler
Serial number: 9011A

Additional information:
This crystal sensor is available in the DCT-lab at the TU/e.
More information can be found in [4].

D.2 Air bearing

Manufacturer: Fabreeka
Serial number: Not available
Vertical damping (adjustable): maximum of 9 percent
Minimal air pressure: 2 bar
Maximal air pressure: 7 bar
Maximal weight load: 339 kg

Additional information:
These air bearings are also used as on the experimental setup of Niels Mallon in the DCT-lab at TU/e. All details are copied from the air bearing characteristics of that experimental setup. The dimensions are not known precisely, because the construction drawings could not be found.

D.3 Roll bearing

Manufacturer: SKF
Serial number: LBBR 8
Inside diameter F_w: 8 mm
Outside diameter D: 15 mm
Length C: 24 mm
Mass: 0.007 kg
Load (dynamical - static): 490 N - 355 N

Additional information:
The outside diameter tolerance of the linear ball bearings is such that no additional axial fixation is required when the bearings are fitted into a bore with a tolerance J7 or J6. This implies +10 μm or -8 μm tolerance with respect to the outside diameter of 15 mm.

D.4 Compression spring

Manufacturer: Tevema
Serial number: D14110
Thickness d: 6.3 mm
Diameter D: 40 mm
Number of compressable windings N_w: 12.5
Total length L_0: 195 mm
Spring constant C: 20100 N/m
Nominal length S_n: 95 mm
Price category: FB

D.5 Extension spring

Manufacturer: Tevema
Serial number: T32240
Thickness: 1.8 mm
Diameter: 10.2 mm
Total length: 290 mm
Spring constant: 680 N/m
Nominal length: 75 mm
Price category: J

D.6 Linear motor

Manufacturer: Anorad
Serial number: LEM-S-1

Additional information:
One unit needed, magnet channel length 300 mm. See appendix F for detailed information. With the linear motor, the manufacturer supplies a Hall sensor and an overheating prevention sensor.

D.7 Encoder

Manufacturer: Renishaw
Serial number: RGH22

Appendix E

Construction costs of the experimental setup

In the following, an overview of the building costs of the setup is given. For clarity, these costs are treated for each distinct part separately. Some of the prices are estimated[1] in the best possible way, since e.g. manufacturing costs are not known exactly in advance.

Linear motor, Anorad LEM-S-1

• Coil	€ 405
• Magnet channel	€ 525
• Thermistor (to prevent overheating)	€ 95
• Amplifier	€ 1500[1]

Measurement instruments

• Encoder strip Renishaw RGH22	€ 67
• Encoder head Renishaw RGH22	€ 350
• Hall sensor Anorad	€ 170

Mass guidance

• Air bearing, 6 pieces	€ 900
• Pressure supply	€ 100[1]
• Air bearing tubing	€ 30[1]
• Lightened, polished triangular body	€ 3000[1]

[1] Estimated price.

Springs

- Extension spring Tevema T32240, only per 5 pieces € 29
- Compression spring Tevema D14110, only per 5 pieces € 29

Miscellaneous

- Ball bearing SKF LBBR8 (stopper) 2 pieces € 100[1]
- Various aluminum parts € 100[1]
- Protection cover € 50[1]

- **Total costs** € 7500[1]

Appendix F

Details about linear motor Anorad LEM-S-1

LEM Brushless Linear Motor

Product Features

- Low force, epoxy core
- Integrated cooling for high duty cycle
- No cogging, no magnetic attraction
- Miniature design
- Ideal for high precision/smooth motion

Specifications

Performance Parameters	Symbol	Units	LEM-S-1			LEM-S-2-S			LEM-S-3-S			LEM-S-4-S		
Cooling Method			NC	AC	WC	NC	AC	WC	NC	AC	WC	NC	AC	WC
Continuous Force [1,5,6,7]	F_{cTmax}	N (lb$_f$)	26 (6)	31 (7)	33 (7)	52 (12)	61 (14)	66 (15)	75 (17)	87 (20)	95 (21)	96 (22)	113 (25)	121 (27)
Peak Force [2]	F_p	N (lb$_f$)	83 (19)	83 (19)	83 (19)	165 (37)	165 (37)	165 (37)	238 (53)	238 (53)	238 (53)	302 (68)	302 (68)	302 (68)
Motor Constant [1]	K_M	N/√W (lb$_f$/√W)	3.9 (0.9)	3.9 (0.9)	3.9 (0.9)	5.8 (1.3)	5.8 (1.3)	5.8 (1.3)	7.1 (1.6)	7.1 (1.6)	7.1 (1.6)	8.2 (1.8)	8.2 (1.8)	8.2 (1.8)
Thermal Resistance	R_{th}	°C/W	2.22	1.63	1.39	1.22	0.90	0.78	0.89	0.66	0.56	0.73	0.53	0.46
Max Power Dissipation	P_{cTmax}	W	45	62	72	82	111	129	113	152	177	136	190	217
Maximum Applied Bus Voltage	V_{DC}	Volts	325			325			325			325		
Electrical Cycle Length	E_c	mm	30			30			30			30		
Electrical Time Constant	τ_e	msec	0.5			0.5			0.5			0.5		
Maximum Coil Temperature	T_{max}	°C	125			125			125			125		
Force Constant [1,8]	K_F	N/A_{pk} (lb$_f$/A_{pk})	5.3 (1.2)	5.3 (1.2)	5.3 (1.2)	11.0 (2.5)	11.0 (2.5)	11.0 (2.5)	16.7 (3.7)	16.7 (3.7)	16.7 (3.7)	22.2 (5.0)	22.2 (5.0)	22.2 (5.0)
Back EMF Constant p-p [3,4,8]	K_e	V_p/m/s (V_p/in/s)	6.3 (0.16)	6.3 (0.16)	6.3 (0.16)	13.0 (0.33)	13.0 (0.33)	13.0 (0.33)	19.7 (0.50)	19.7 (0.50)	19.7 (0.50)	26.3 (0.67)	26.3 (0.67)	26.3 (0.67)
Peak Current [1,4]	I_p	A_{pk} (A_{rms})	15.6 (11.0)	15.6 (11.0)	15.6 (11.0)	15.0 (10.6)	15.0 (10.6)	15.0 (10.6)	14.3 (10.1)	14.3 (10.1)	14.3 (10.1)	13.6 (9.6)	13.6 (9.6)	13.6 (9.6)
Continuous Current [1,4,5,6]	I_{cTmax}	A_{pk} (A_{rms})	4.9 (3.5)	5.8 (4.1)	6.3 (4.4)	4.8 (3.4)	5.5 (3.9)	6.0 (4.2)	4.5 (3.2)	5.2 (3.7)	5.7 (4.0)	4.3 (3.1)	5.1 (3.6)	5.4 (3.9)
Resistance p-p [3,8] @25°C	R_{25}	ohm	1.8			3.5			5.3			7.1		
Inductance p-p [3]	L	mH	0.9			1.8			2.7			3.6		
Mechanical Parameters														
Magnetic Attraction	F_a	N (lb$_f$)	0 (0)			0 (0)			0 (0)			0 (0)		
Coil Mass [5]	M_c	kg (lb$_m$)	0.2 (0.3)	0.2 (0.3)	0.2 (0.3)	0.3 (0.7)	0.3 (0.7)	0.3 (0.7)	0.5 (1.0)	0.5 (1.0)	0.5 (1.0)	0.6 (1.4)	0.6 (1.4)	0.6 (1.4)
Magnetic Track Mass	M_a	kg/m (lb/in)	5.2 (0.29)			5.2 (0.29)			5.2 (0.29)			5.2 (0.29)		
Cooling Flow Rate	Q	LPM (SCFM/GPM)	n/a (n/a)	113.0 (3.9)	4.0 (1.1)	n/a (n/a)	108.0 (3.7)	4.0 (1.1)	n/a (n/a)	102.0 (3.5)	4.0 (1.1)	n/a (n/a)	93.0 (3.0)	4.0 (1.1)
Cooling Supply Pressure	P	kPa (PSIG)	n/a (n/a)	207 (30)	179 (26)	n/a (n/a)	207 (30)	193 (28)	n/a (n/a)	207 (30)	207 (30)	n/a (n/a)	207 (30)	276 (40)

Notes: Motor performance specifications are with sinusoidal commutation.

[1] Continuous forces, motor constant and currents listed are with coils at maximum temperature 125°C, mounted to a 254 x 254 x 25.4 mm (10" x 10" x 1") aluminum heat sink on top of coil, and at 25°C ambient.

[2] Max on time 1 sec., assuming correct rms Force and Current, consult Anorad.

[3] All winding parameters listed are measured line-to-line (phase-to-phase).

[4] All currents and voltages listed are measured 0-peak of the sine wave unless noted rms.

[5] Continuous forces and currents are also based on coil moving with all phases sharing the same load in sinusoidal commutation.

[6] For stand still conditions multiply continuous force and continuous current by 0.9.

[7] Coil mountings on either of the two narrow sides reduces continuous force by 20%.

[8] All specifications are ±10%.

LEM Brushless Linear Motor

Product Features

- Low force, epoxy core
- Integrated cooling for high duty cycle
- No cogging, no magnetic attraction
- Miniature design
- Ideal for high precision/smooth motion

Specifications

Performance Parameters	Symbol	Units	LEM-S-1			LEM-S-2-S			LEM-S-3-S			LEM-S-4-S		
Cooling Method			NC	AC	WC	NC	AC	WC	NC	AC	WC	NC	AC	WC
Continuous Force [1,5,6,7]	F_{cTmax}	N (lb_f)	26 (6)	31 (7)	33 (7)	52 (12)	61 (14)	66 (15)	75 (17)	87 (20)	95 (21)	96 (22)	113 (25)	121 (27)
Peak Force [2]	F_p	N (lb_f)	83 (19)	83 (19)	83 (19)	165 (37)	165 (37)	165 (37)	238 (53)	238 (53)	238 (53)	302 (68)	302 (68)	302 (68)
Motor Constant [1]	K_M	N/√W (lb_f/√W)	3.9 (0.9)	3.9 (0.9)	3.9 (0.9)	5.8 (1.3)	5.8 (1.3)	5.8 (1.3)	7.1 (1.6)	7.1 (1.6)	7.1 (1.6)	8.2 (1.8)	8.2 (1.8)	8.2 (1.8)
Thermal Resistance	R_{th}	°C/W	2.22	1.63	1.39	1.22	0.90	0.78	0.89	0.66	0.56	0.73	0.53	0.46
Max Power Dissipation	P_{cTmax}	W	45	62	72	82	111	129	113	152	177	136	190	217
Maximum Applied Bus Voltage	V_{DC}	Volts	325			325			325			325		
Electrical Cycle Length	E_c	mm	30			30			30			30		
Electrical Time Constant	τ_e	msec	0.5			0.5			0.5			0.5		
Maximum Coil Temperature	T_{max}	°C	125			125			125			125		
Force Constant [1,8]	K_F	N/A_{pk} (lb_f/A_{pk})	5.3 (1.2)	5.3 (1.2)	5.3 (1.2)	11.0 (2.5)	11.0 (2.5)	11.0 (2.5)	16.7 (3.7)	16.7 (3.7)	16.7 (3.7)	22.2 (5.0)	22.2 (5.0)	22.2 (5.0)
Back EMF Constant p-p [3,4,8]	K_e	V_p/m/s (V_p/in/s)	6.3 (0.16)	6.3 (0.16)	6.3 (0.16)	13.0 (0.33)	13.0 (0.33)	13.0 (0.33)	19.7 (0.50)	19.7 (0.50)	19.7 (0.50)	26.3 (0.67)	26.3 (0.67)	26.3 (0.67)
Peak Current [1,4]	I_p	A_{pk} (A_{rms})	15.6 (11.0)	15.6 (11.0)	15.6 (11.0)	15.0 (10.6)	15.0 (10.6)	15.0 (10.6)	14.3 (10.1)	14.3 (10.1)	14.3 (10.1)	13.6 (9.6)	13.6 (9.6)	13.6 (9.6)
Continuous Current [1,4,5,6]	I_{cTmax}	A_{pk} (A_{rms})	4.9 (3.5)	5.8 (4.1)	6.3 (4.4)	4.8 (3.4)	5.5 (3.9)	6.0 (4.2)	4.5 (3.2)	5.2 (3.7)	5.7 (4.0)	4.3 (3.1)	5.1 (3.6)	5.4 (3.9)
Resistance p-p [3,8] @25°C	R_{25}	ohm	1.8			3.5			5.3			7.1		
Inductance p-p [3]	L	mH	0.9			1.8			2.7			3.6		
Mechanical Parameters														
Magnetic Attraction	F_a	N (lb_f)	0 (0)			0 (0)			0 (0)			0 (0)		
Coil Mass [5]	M_c	kg (lb_m)	0.2 (0.3)	0.2 (0.3)	0.2 (0.3)	0.3 (0.7)	0.3 (0.7)	0.3 (0.7)	0.5 (1.0)	0.5 (1.0)	0.5 (1.0)	0.6 (1.4)	0.6 (1.4)	0.6 (1.4)
Magnetic Track Mass	M_n	kg/m (lb/in)	5.2 (0.29)			5.2 (0.29)			5.2 (0.29)			5.2 (0.29)		
Cooling Flow Rate	Q	LPM (SCFM/GPM)	n/a (n/a)	113.0 (3.9)	4.0 (1.1)	n/a (n/a)	108.0 (3.7)	4.0 (1.1)	n/a (n/a)	102.0 (3.5)	4.0 (1.1)	n/a (n/a)	93.0 (3.0)	4.0 (1.1)
Cooling Supply Pressure	P	kPa (PSIG)	n/a (n/a)	207 (30)	179 (26)	n/a (n/a)	207 (30)	193 (28)	n/a (n/a)	207 (30)	207 (30)	n/a (n/a)	207 (30)	276 (40)

Notes: Motor performance specifications are with sinusoidal commutation.

[1] Continuous forces, motor constant and currents listed are with coils at maximum temperature 125°C, mounted to a 254 x 254 x 25.4 mm (10" x 10" x 1") aluminum heat sink on top of coil, and at 25°C ambient.

[2] Max on time 1 sec., assuming correct rms Force and Current, consult Anorad.

[3] All winding parameters listed are measured line-to-line (phase-to-phase).

[4] All currents and voltages listed are measured 0-peak of the sine wave unless noted rms.

[5] Continuous forces and currents are also based on coil moving with all phases sharing the same load in sinusoidal commutation.

[6] For stand still conditions multiply continuous force and continuous current by 0.9.

[7] Coil mountings on either of the two narrow sides reduces continuous force by 20%.

[8] All specifications are ±10%.

Copied from [5].